Presented at the 34th JANNAF Combustion Subcommittee Meeting
West Palm Beach, Florida, October, 1997

Mechanistic and Kinetic Studies of the Thermal Decomposition of TNAZ and NDNAZ*†

Kraig Anderson, Jason Homsy, and Richard Behrens
Combustion Research Facility
Sandia National Laboratories
Livermore, CA 94551

Suryanarayana Bulusu‡
Energetic Materials Division
U.S. Army Armament Research, Development and Engineering Center
Dover, NJ 07801-5001

ABSTRACT

We have studied the mechanism and detailed reaction kinetics of the thermal decomposition of 1,3,3-trinitroazetidine (TNAZ), and separately, its key decomposition intermediate, 1-nitroso-3,3-dinitroazetidine (NDNAZ), using a simultaneous thermogravimetric modulated beam mass spectrometer (STMBMS). These decompositions were conducted in a sealed alumina cell with a 2.5 μm orifice, at varying temperatures and at a range of isothermal temperatures (at 10°C intervals from 120-160°C for NDNAZ and 160-210°C for TNAZ). The gaseous products have been identified and their rates of formation have been measured as a function of time, temperature, and pressure. This system is complex, with TNAZ decomposing by four separate routes, one of which leads to NDNAZ, which itself decomposes by at least two distinct routes.

INTRODUCTION

The new energetic material TNAZ (1,3,3-trinitroazetidine),[1] alone and as a eutectic with the closely related NDNAZ (1-nitroso-3,3-dinitroazetidine), has been under serious consideration as a relatively insensitive, high energy, melt castable replacement for HMX and TNT. We therefore began a detailed analysis of the kinetics and mechanisms of their thermal decomposition behaviors in order to develop a predictive model which will be useful in planning appropriate processing, storage, and usage conditions for these new materials. Additionally, we have a great deal of interest in TNAZ as a cyclic nitramine arising from our past detailed work on RDX and HMX.[2-16]

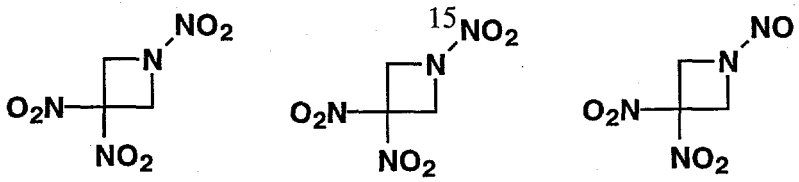

TNAZ N-$^{15}NO_2$TNAZ NDNAZ

Previous work by other groups examined TNAZ decomposition in the condensed phase, by rapid-scan Fourier transform infrared spectroscopy (RSFTIR),[17] and in a molecular beam, by infrared multiphoton dissociation (IRMPD).[18] Both studies showed NO_2 loss by cleavage of either the nitramine or a nitroalkane group. The condensed-phase work also indicated HNO_2 elimination and nitro-nitrite rearrangement of the nitroalkane groups. The molecular beam work suggested that the initial NO_2 cleavage was followed by ring-opening, additional NO_2 loss and then decomposition to N_2O_2 and C_3H_4. Neither study determined which, or if both, of the nitramine and nitroalkane groups were responsible for the initial NO_2 cleavage. It is unclear whether the unimolecular processes operant in the molecular beam environment also control decomposition in higher pressure environments, or if bimolecular processes are important. Also, in the condensed phase study, the existence of the nitro-nitrite rearrangement was uncertain, and the observation of HONO suggested the possibility of an alternative decomposition pathway to NO_2 cleavage.

---

* Approved for public release; distribution is unlimited.

† Work supported by the Army Research Office, a Memorandum of Understanding between the U.S. Department of Energy and the Office of Munitions and by the U.S. Department of Energy under contract DE-AC04-94AL85000.

‡ Deceased.

DISCLAIMER

In preliminary work reported previously,[19, 20] we identified the major liquid/gas phase thermal decomposition products of TNAZ. One important new product we observed is its nitroso analog, NDNAZ, which we anticipated based on our previous observations of nitroso analogs formed in the decomposition of other cyclic nitramines such as HMX and RDX. We also reported the major thermal decomposition products of independently-synthesized NDNAZ, and, using N-$^{15}NO_2$ labelled TNAZ, showed that NO_2 loss occurs at both possible sites with cleavage of the weaker nitramine bond preceding that of the gem-dinitroalkane group. Here we report additional mechanistic details, improved experimental techniques, gas formation rates of major decomposition species versus time, and a novel autocatalytic behavior displayed by a polymeric decomposition residue.

EXPERIMENTAL

The experiments for this report were conducted using our Simultaneous Thermogravimetric Modulated Beam Mass Spectrometer (STMBMS), which we have described in detail previously.[21-23] Briefly, samples of energetic material (ca. 5-15 mg) are loaded into an alumina reaction cell (internal volume ~ 0.25 cc) containing a "splash" baffle and capped with a supported gold foil disk with a small orifice. The orifice size can be varied to choose the amount of containment of evaporated TNAZ/NDNAZ and evolved gaseous decomposition products. The cell is loaded onto a thermocouple probe attached to the arm of a microbalance. The reaction cell is surrounded by a tubular alumina furnace shell wrapped with a bifilar-wound tungsten wire heating element. During an experiment, the chamber is evacuated to ~1 X 10^{-6} Torr. The effluent from the cell undergoes an isentropic expansion, passes through two beam-defining orifices located in a differentially-pumped vacuum chamber, and is chopped by a rotating, toothed wheel. This modulated beam enters a quadrupole mass spectrometer, which gains a considerable improvement in the signal-to-noise ratio by subtracting the background signal from the signal of the free beam. Ions are generated in the mass spectrometer by electron impact at an energy of ~20 eV, less than the typical ~70 eV in order to reduce the contribution of ion fragmentation due to electron impact. Mass spectra, weight loss, and temperature data are collected versus time. By correlating the ion signals with the force measured by the microbalance, the concentration and formation rate of each gaseous decomposition product can be determined.

We have made several improvements in our experimental design. We have extended the range of gas containment, going down to orifice sizes as small as 2.5 μm. The gold orifice disk is compressed on top of an O-ring residing in a recessed groove in the tapered alumina cap, and a light coat of silicone vacuum grease seals the tapered joint between the cap and the cell; no significant weight loss or ion signal contribution due to the silicone grease is observed in the temperature range of this study. Under these conditions pressures exceeding 1000 Torr can be achieved during a NDNAZ or TNAZ experiment.

The flow through such small, irregularly shaped channels is not amenable to an analytic description. We have dealt with this in the past for larger orifices by calibrating the weight loss and ion signal of a naphthalene evaporation experiment to literature vapor pressure data. These calibrations, however, are time consuming and thus impractical for continuing surveillance of orifice flow characteristics which can change dramatically upon deposition of a miniscule amount of material. Therefore, we devised a rapid flow test, separate from the STMBMS, consisting of a measured, minimum volume, stainless steel dummy cell equipped with a pressure transducer and appropriate valving. A known amount of N_2 is applied to one side of the orifice and an active vacuum to the other. The pressure drop as the N_2 flows through the orifice is measured versus time. From this, the relationship between flow rate and pressure is determined, and furthermore, the question of whether the flow characteristics of a particular orifice have changed after an experiment can be answered. One naphthalene calibration experiment is run for each 2.5 μm orifice and is assumed valid as long as the N_2 flow tests for that orifice do not vary significantly.

The extent of gas containment is determined by the flow characteristics of the orifice (which vary among orifices of the same nominal size), the free volume of the cell (fixed in this study), and the leak rate of the cell. For 2.5 μm experiments, we demand the leak rate at a cell pressure of 1000 Torr, measured before and after the experiment with a helium leak detector, be less than 1% of the flow rate through the orifice. Typical flow rates at 1000 Torr for nominally 2.5 μm orifices range from 4.0-9.0 X 10^{-8} mol/s. Cell leak rates of 2.0 X 10^{-10} mol/s are routinely achievable and cells with a carefully matched cap can have rates as low as 5 X 10^{-12} mol/s. These rates are usually the same or smaller after an experiment; in rare cases where the cell seal fails, there are obvious residue streaks around the cap.

Successful use of the 2.5 μm orifices is quite challenging. They are actually channels rather than point orifices (the gold foil is 25 μm thick), and are quite rough compared to their diameter (Figure 1). Because the volume of the orifice channel is only ~5 X 10^{-10} cm^3, full obstruction of the orifice would require only a few picomoles or roughly $1/10^7$ of a typical sample! Considering that most of the materials we study are prone to forming intractable polymeric residues, it is quite remarkable these orifices are useful at all.

Syntheses of TNAZ and $^{15}NO_2$-TNAZ have been previously described.[19, 20] Samples of NDNAZ were obtained from M. Hiskey at Los Alamos National Laboratory. A final purification to remove adsorbed water and small amounts of other volatile impurities was performed by holding the reactions at an initial isotherm of 100°C for 3000-5000 seconds.

Data analysis and quantification techniques have been described in detail elsewhere.[21-23] In our earlier report, we described preliminary decomposition experiments primarily conducted with a linear heating ramp and a few high temperature, isothermal experiments. The interpretations were based on the raw ion signal data, which can be misleading because the absolute ion signals depend on the ion formation probabilities of the parent molecules. Here we present data from isothermal experiments conducted at 10°C increments spanning 120-160°C for NDNAZ and 160-210°C for TNAZ. The raw data have been corrected to reflect the relative ion formation probabilities of the species measured.

RESULTS AND DISCUSSION

TNAZ DECOMPOSITION

Previously we reported the major decomposition products of TNAZ were NO and NO_2, based on ion signal intensities. We find that NO and NO_2 are still major decomposition products after adjusting for relative ion formation probabilities, although the latter's importance is substantially reduced, especially at higher temperatures. This adjustment also reveals a more significant role for products such as H_2O and CO/N_2, and to a lesser extent CO_2/N_2O, HCN, and CH_2O. At low temperatures, the major initial product is NO_2 (Figure 2). At higher temperatures, the relative amount of NO_2 is decreased and the relative amount of NO is increased. At higher temperatures, H_2O, CO/N_2, CO_2/N_2O, and HCN also become more important (not shown). A smaller, yet significant product is the N-nitroso analog of TNAZ, NDNAZ (Figure 3). On increasing temperature, its amount and gas formation rate decrease relative to the other products, which is reasonable since it decomposes much more readily than TNAZ. The time evolution changes, however, with the initial gas formation rate rising earlier with increasing temperature, following the increase in NO. Also notable are small increases in the gas formation rates of several decomposition products following the increase in NDNAZ, which correspond to products of its decomposition.

Experiments using N-$^{15}NO_2$ labeled TNAZ show both isotopes are represented in NO and NO_2, proving they are from both the nitramine and the gem-dinitroalkane sites (Figure 2). Because their gas formation rates, though similar at low temperatures, are not perfectly correlated and diverge further with increasing temperature, they must be generated by different reaction pathways. The relative gas formation rates of $^{15}NO_2$ are much greater than for $^{14}NO_2$, starting at a ratio of approximately 16:1 at 160°C and decreasing to about 6:1 at 210°C. As this ratio decreases with elevated temperature, the gas formation rate of ^{15}NO increases, particularly the initial rate. At low temperatures, the ^{14}NO gas formation rate is about 20% greater than for ^{15}NO over the course of the decomposition, with similar (though not perfectly correlated) time evolutions for each showing a gradual decline from the initial peak rate. At 210°C, the initial formation rate of ^{15}NO is nearly double that of ^{14}NO but decreases fairly rapidly, contrary to the ^{14}NO rate which increases more slowly and holds relatively constant for some time after reaching its peak. These behaviors indicate the first decomposition step is cleavage of the nitramine $^{15}NO_2$ group. This is followed by a temperature sensitive decomposition of the free $^{15}NO_2$, generating most or all of the observed ^{15}NO. In contrast, relatively little $^{14}NO_2$ arises from the gem-dinitroalkane group at any temperature. Because there is still a considerable amount of ^{14}NO, however, it must be produced by mechanisms other than free $^{14}NO_2$ decomposition. The primary mechanism is probably nitro-nitrite rearrangement of the gem-dinitroalkane followed by decomposition to ^{14}NO, CO_2, and other fragments.

Also interesting is the lack of correlation between the ^{15}NO-NDNAZ and ^{14}NO-NDNAZ (Figure 3). These are somewhat similar at low temperatures, but at higher temperatures they become quite different, with the ^{15}NO-NDNAZ formation rate rising significantly earlier in the course of the decomposition. The difference is not as great as that between ^{14}NO and ^{15}NO but the two sets of products do compare. Because the ^{15}NO-NDNAZ rate decreases as ^{15}NO decreases while the ^{14}NO-NDNAZ drops when the TNAZ signal drops, we surmise that NDNAZ formation is dependent on NO concentration, and furthermore, it occurs primarily by a direct displacement of the nitramine-NO_2 group by NO.

NDNAZ DECOMPOSITION

We also performed a series of experiments using independently synthesized NDNAZ. The number of pathways important in NDNAZ decomposition seems to be less than for TNAZ, though the entire process is still complex. The product mix is substantially different, however, and the decomposition, which proceeds more readily, also exhibits a dramatic autocatalytic effect.

The major product is again NO, which must come from both the nitrosamine and the gem-dinitroalkane sites because more than one equivalent of NO is released (Figure 4). Although we have not examined labeled NDNAZ, several observations point to nitrosamine cleavage as the likely dominant source of NO in the initial, precatalysis phase. First, the nitrosamine bond is weaker than the gem-dinitroalkane bond. Second, simple cleavage is sufficient to release NO from the nitrosamine site, wheras a more complicated (and presumably slower) pathway is required to generate NO from the gem-dinitroalkane site. Third, low levels of NO_2 show nitroalkane cleavage followed by decomposition to NO (probably the simplest potential route to NO from the gem-dinitroalkane) is not an important reaction, which is also consistent with observations of TNAZ decomposition. Fourth, because the gas formation rate of NO is greater relative to other low molecular weight products in the initial phase, it must be dominated by a process like nitrosamine cleavage which releases NO and a high molecular weight, low volatility species.

The advent of pathways generating low molecular weight products in addition to NO are consistent with the increasing importance of low molecular weight gaseous products relative to NO in the catalysis phase. An obvious candidate is a pathway involving nitro-nitrite rearrangement as observed in TNAZ decomposition, which generates CO_2 and other products upon releasing NO.

A minor, but significant product due to its high molecular weight, is observed at m/z 131. One plausible route to a product at m/z 131 is shown in Scheme 1. Initial steps involve nitrosamine cleavage, hydrogen addition, and at least one nitro-nitrite rearrangement. The key step is the decomposition of an alkyl nitrite to NO and the corresponding alcohol in the presence of water. Elimination to the alkene is next, followed by NO addition to the double bond and another hydrogen addition to give a m/z = 131 species. The actual sequence of steps may vary, and there is as yet no direct proof of the structure at m/z 131. Given the the high concentrations of NO and H_2O, however, and that nitrosamine cleavage and nitro-nitrite rearrangements are already favored, we feel this scheme is reasonable. Future studies will use isotopically labeled NDNAZ to further investigate this mechanism.

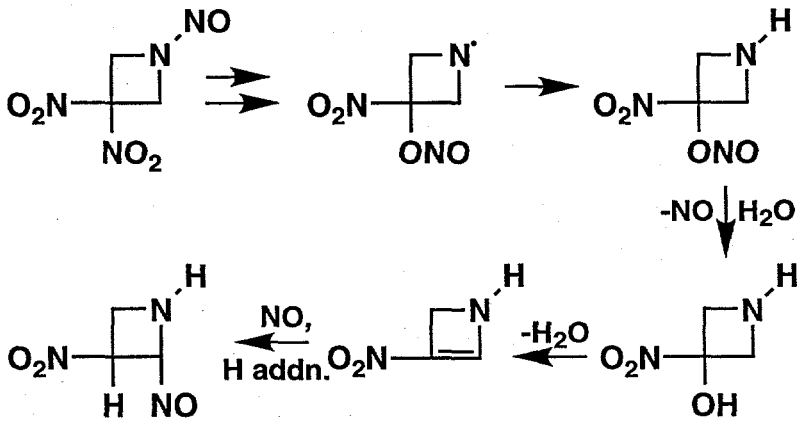

Scheme 1: Possible reaction path leading to a species at m/z 131.

The key feature of NDNAZ decomposition is the autocatalysis exhibited after an initial induction period. This leads to a substantial rise in gas formation rates, nearly 400% in the case of NO formation at a 150°C isotherm. We have observed similar behavior for other compounds, which like NDNAZ, form polymeric residues. Proof of the catalytic activity of the polymer residue is given by an experiment (Figure 5) where fresh NDNAZ was added to the residue-coated cell from a prior NDNAZ decomposition. Upon heating to the same isotherm, formation rates of the decomposition products rose almost immediately to the high rates seen near the end of the catalysis phase of the previous experiment.

Is this residue a general catalyst or specific to NDNAZ? The TNAZ decomposition experiments show a slight rise in product formation rates near the end. This rise is due at least to NDNAZ decomposition. It is possible that residue-catalyzed NDNAZ and TNAZ decomposition also contribute to this feature. It is also true, however, that TNAZ forms much less residue than NDNAZ, so there may not be enough to have a clear effect. An obvious future experiment is to add fresh TNAZ to a cell coated with NDNAZ residue.

In this sort of catalysis, one likely controlling feature is surface area. When we required samples of these intractable residues for elemental analysis, we tried adding clean, microscopic (~100 μm) glass beads to the reaction cell, hoping the residue would coat the beads and could then be easily removed from the cell. Although effective for its intended purpose, this also led to observable autocatalysis in *both* TNAZ and NDNAZ decompositions; furthermore, the effect was much more dramatic than in experiments without glass beads (Figure 6). Certainly, simply increasing available surface area can give a catalytic effect. When the rate of catalysis (in an isothermal experiment) increases with the reaction progress, however, it clearly indicates the role of an accumulating product, the definition of autocatalysis. The increase in the catalytic effect compared to experiments without beads suggests the beads serve at least to increase the surface area available for a catalytic residue, but does not rule out a participating catalytic role for the surface of the beads.

One feature shown by both TNAZ and NDNAZ is duration of product evolution after the parent molecule is depleted (Figure 7). At low temperatures, product evolution drops almost as soon as the parent is depleted. At higher temperatures, products continue to evolve after depletion. This indicates the formation of less volatile, higher MW products, such as the polymeric residue, or containment of volatile products within the residue. Consistent with the amount of polymeric residue formed for each material, the continued evolution of products after depletion is more important in NDNAZ decomposition than in TNAZ decomposition.

TNAZ DECOMPOSITION PATHWAYS

The basic framework of TNAZ decomposition is shown below (Scheme 2). Clearly, the first and most important step is cleavage of the nitramine bond, releasing NO_2 and the 3,3-dinitroazetidinyl radical. Cleavage of a gem-dinitroalkane occurs, but to a substantially lesser degree. Another important route is the nitro-nitrite rearrangement. All of these routes lead to NO formation, which in turn leads to a direct displacement of the nitramine NO_2 groups on remaining TNAZ molecules. Another possible path is elimination of $HONO/HNO_2$ (not shown), but this does not seem to be an important pathway.

NDNAZ DECOMPOSITION PATHWAYS

There are two likely first steps for the decomposition of NDNAZ. The first involves cleavage of the nitrosamine bond, which as discussed before, is probably the dominant process in the initial, precatalysis phase. The other likely pathway begins with the nitro-nitrite rearrangement. Because the amount of NO relative to the other decomposition products is much larger than in the TNAZ decomposition, in fact larger than can be accounted for by nitrosamine cleavage, it suggests some feature of NDNAZ or its decomposition environment favors the nitro-nitrite rearrangement, most likely the catalytic polymeric residue. This can be tested by decomposing fresh TNAZ in the presence of the polymeric residue; if true, the relative amounts of NO production would be much higher than for TNAZ decomposition alone. Other possible first steps, such as direct NO_2 cleavage or $HONO/HNO_2$ elimination, may be present in small amounts but are not major contributors according to the data.

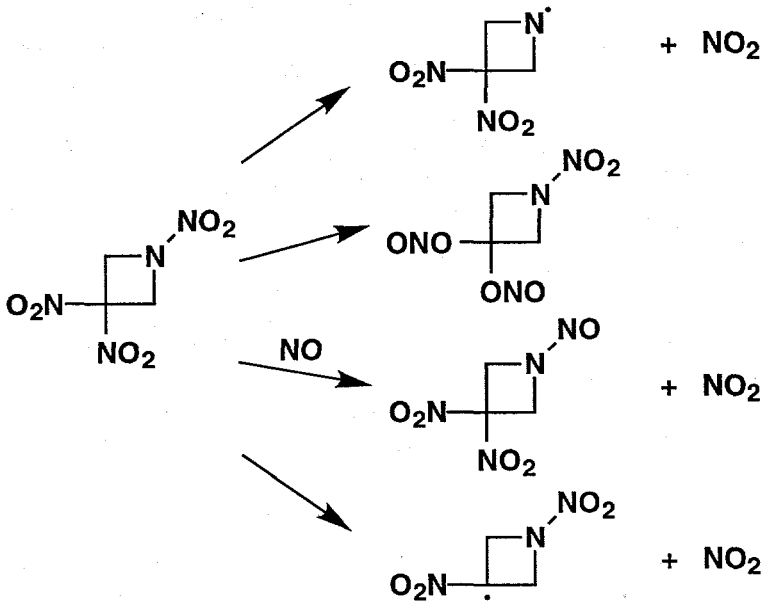

Scheme 2: Major TNAZ decomposition pathways

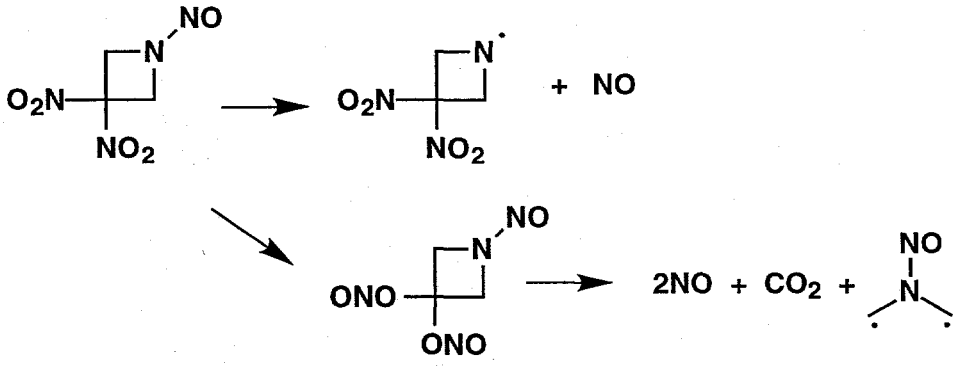

Scheme 3: Major NDNAZ decomposition pathways

FUTURE WORK

Work continues on this system to complete collection of quantitative data and address a few more mechanistic details, such as the structure, formation, and activity of the catalytic polymer residue from NDNAZ. Time-of-flight velocity spectra will be employed to identify which minor peaks are actually products and not fragments of parent molecules created by electron impact ionization in the quadrupole mass spectrometer employed in this study. This information will be folded into a global decomposition model incorporating the different reaction pathways, the quantified data, and the gas formation rates.

SUMMARY

The major products formed in the decomposition of TNAZ are NO_2 and NO, with lesser amounts of H_2O, HCN, CO/N_2, CO_2/N_2O, NDNAZ, and a small amount of polymeric residue. The results indicate four likely steps for the first step in the TNAZ decomposition. Three of these generate NO_2, either by unimolecular cleavage of a nitramine or nitroalkane, or by displacement of the nitramine NO_2 by NO, while the fourth involves a nitro-nitrite rearrangement of the gem-dinitro group (elimination of HNO_2 occurs, but is relatively small). The unimolecular fragmentation pathways are supported because NO_2 generation is initially first order in TNAZ concentration in both liquid and gas phases (additional sources of NO_2 must exist because its signal does not decrease as TNAZ nears

depletion). Experiments using 1-$^{15}NO_2$-TNAZ show NO_2 evolution from both sites in the molecule, though occuring first at the weaker nitramine bond; and also indicate, by lack of isotopic shifts, that signals at m/z 28 and 44 are mostly CO and CO_2 rather than N_2 and N_2O. The observation that the rates of formation of NO_2, NO, and NDNAZ increase sequentially indicates NDNAZ is formed by direct replacement of the nitramine NO_2 in TNAZ by NO. This and the nitro-nitrite pathway are also suggested because CO_2, NO, CO/N_2, HCN, CH_3CN, and NDNAZ do not correlate with the first-order NO_2 cleavage. Evolution of CO_2/N_2O, NO, HCN, and CO/N_2 after TNAZ depletion indicates they are thermal decomposition products of NDNAZ.

The decomposition of independently synthesized NDNAZ provides further clues to the overall decomposition process. The major product in the decomposition of NDNAZ is NO, followed by lesser amounts of H_2O, HCN, CO/N_2, CO_2/N_2O, and a significant amount of polymeric residue, which actually catalyzes NDNAZ decomposition. While these products are similar to those formed in the TNAZ decomposition, their ratios differ significantly. There are two likely first steps for the decomposition of NDNAZ, either cleavage of the N-nitroso group to form NO and 3,3-dinitroaziridinyl radical, or nitro-nitrite rearrangement of the gem-dinitro group. Because more than one equivalent of NO is evolved, a nitro-nitrite rearrangement as in the second path almost certainly occurs.

The results of our experiments confirm loss of NO_2 as one of the first steps in TNAZ decomposition, as discovered in RSFTIR and IRMPD experiments by other groups, and furthermore, show that the NO_2 arises from both possible sites. Contrary to the RSFTIR experiments, however, HNO_2 elimination is relatively unimportant. We find once again that a mononitroso analog (NDNAZ) is an important intermediate in nitramine decomposition, as we have shown previously for RDX, TNCHP, and HMX.

Several significant improvements have been made to our experimental protocol, allowing the effective use and characterization of 2.5 μm diameter orifices, despite their inherent difficulties. With these improvements, quantification of our data is more reliable. Coupled with kinetic, mechanistic, and physical information on these decompositions, this will provide the foundation to develop a detailed mathematical model of the decomposition processes of TNAZ and NDNAZ.

ACKNOWLEDGMENTS

We thank D.M. Puckett for collecting the mass spectrometry data and to Dr. Michael Hiskey for providing the 2,4-DNI sample. Work is supported by the Army Research Office, a Memorandum of Understanding between the DoD Office of Munitions and the Department of Energy under Contract DE-AC04-94AL85000, and by the U.S. Army, ARDEC.

REFERENCES

1 T. G. Archibald, R. Gilardi, K. Baum, *et al.*, Journal of Organic Chemistry **55**, 2920 (1990).

2 R. Behrens, Jr. and S. Bulusu, Journal of Physical Chemistry **96**, 8891-8897 (1992).

3 R. Behrens, Jr. and S. Bulusu, Journal of Physical Chemistry **96**, 8877-8891 (1992).

4 R. Behrens, Jr. and S. Bulusu, in *29th JANNAF Combustion Meeting* (Chemical Propulsion Information Agency, Langley, Virginia, 1992).

5 R. Behrens, Jr. and S. Bulusu, Journal of Physical Chemistry **96**, 8891-8897 (1992).

6 R. Behrens, Jr. and S. Bulusu, Journal of Physical Chemistry **96**, 8877 - 8891 (1992).

7 R. Behrens, Jr. and S. Bulusu, Journal of Physical Chemistry **95**, 5838 (1991).

8 R. Behrens, Jr. and S. Bulusu, Journal of Physical Chemistry **95**, 5838-5845 (1991).

9 R. Behrens, Jr., Journal of Physical Chemistry **94**, 6706-6718 (1990).

10 R. Behrens, Jr., International Journal of Chemical Kinetics **22**, 159-173 (1990).

11 R. Behrens, Jr., International Journal of Chemical Kinetics **22**, 135-157 (1990).

12 R. Behrens, in *Chemistry and Physics of Energetic Materials*, edited by S. N. Bulusu (Kluwer Academic Publishers, Dordrecht, The Netherlands, 1990), Vol. 309, p. 347.

13 R. Behrens, Jr., International Journal of Chemical Kinetics **22**, 159 (1990).

14 R. Behrens, Jr., in *23rd JANNAF Combustion Meeting* (Chemical Propulsion Information Agency, 1986), Vol. 457, p. 231.

15 R. Behrens, Jr., in *24th JANNAF Combustion Meeting* (Chemical Propulsion Information Agency, Monterey, California, 1987), Vol. 476, p. 333-342.

16 R. Behrens, Journal of Physical Chemistry **94**, 6706 (1990).

17 Y. Oyumi and T. B. Brill, Combustion and Flame **62**, 225-231 (1985).

18 D. S. Anex, J. C. Allman, and Y. T. Lee, in *Chemistry of Energetic Materials*, edited by G. A. Olah and D. R. Squires (Academic Press, 1991), p. 27 - 54.

19 R. Behrens and S. Bulusu, Defence Science Journal (India) **46**, 361 - 369 (1996).

20 R. Behrens and S. Bulusu, in *32nd JANNAF Combustion Subcommittee Meeting* (CPIA Publication #638, Huntsville, AL, 1995), Vol. 1, p. 1 - 11.

21 R. Behrens, Jr., Reveiw of Scientific Instruments **58**, 451 (1986).

22 R. Behrens, Jr., Review of Scientific Instruments **58**, 451-461 (1987).

23 R. Behrens, Jr., in *Chemistry and Physics of Energetic Materials*, edited by S. N. Bulusu (Kluwer Academic Publishers, Netherlands, 1990), Vol. 309, p. 327.

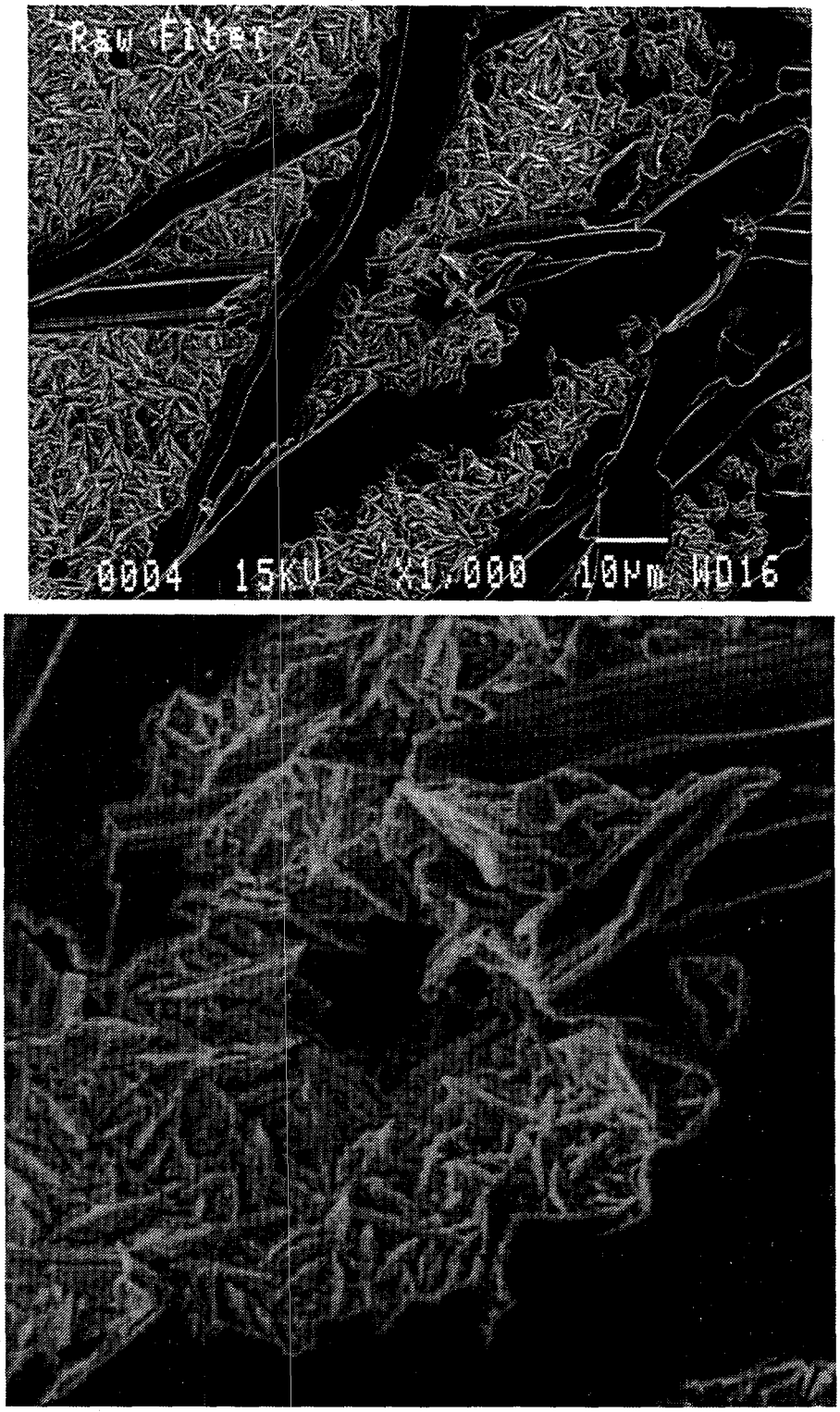

Figure 1: Electron microscope pictures of a 2.5 μm orifice disk. Top (1000X): The orifice is the dark spot in the center, framed by smooth dark bands. These bands are mechanical scratches made to assist location of the orifice under a light microscope. Bottom: Same orifice, higher magnification. The orifice is quite rough and irregular compared to its diameter. The gold in the undisturbed areas appears semicrystalline.

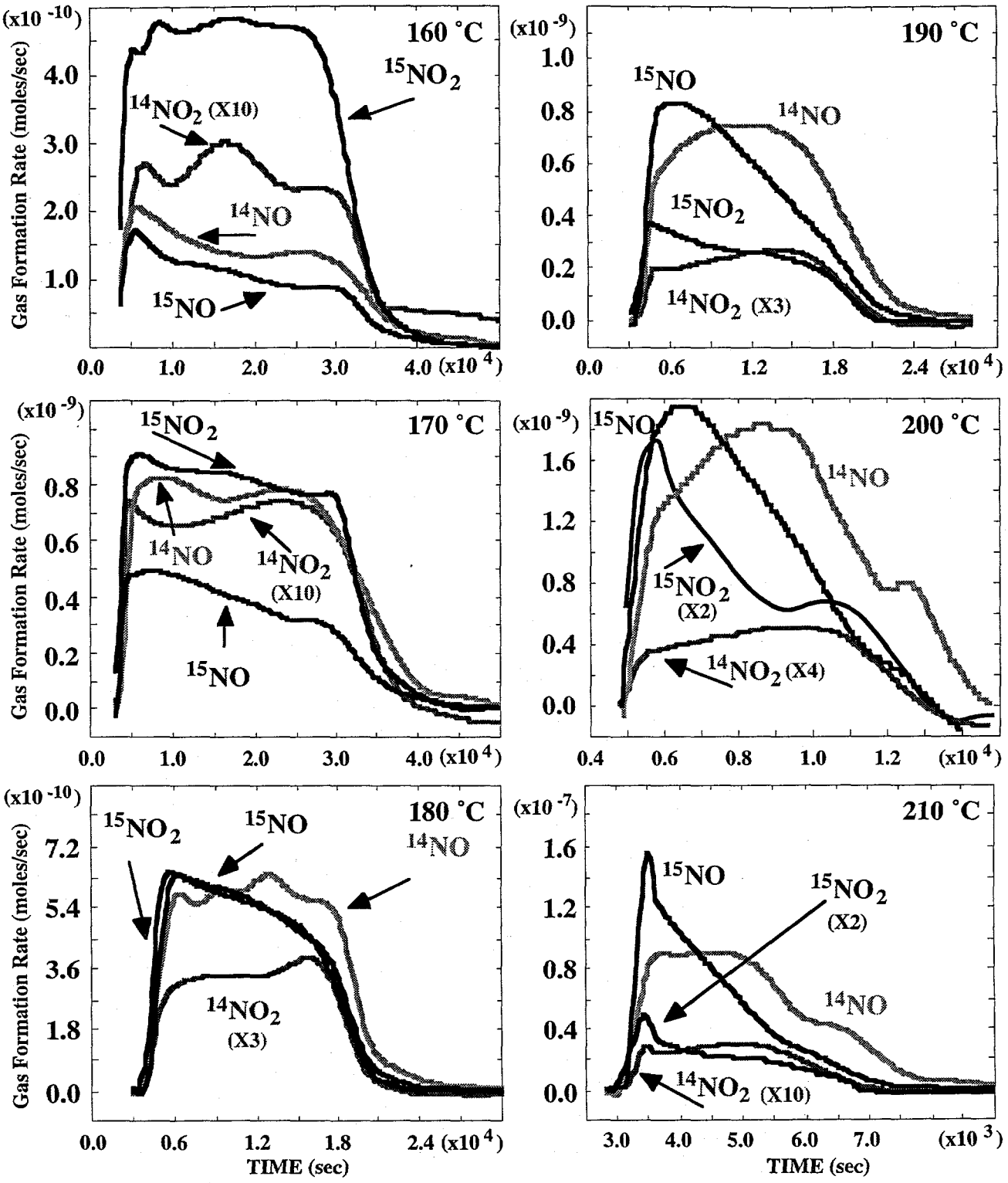

Figure 2: Gas formation rates for ^{14}NO, ^{15}NO, $^{14}NO_2$, and $^{15}NO_2$ in N-$^{15}NO_2$ labeled TNAZ at isotherms from 160-210°C. Initially, $^{15}NO_2$ dominates. Overall, $^{14}NO_2$ lags $^{15}NO_2$ slightly. At high temperature, $^{14/15}NO$ dominates, with ^{15}NO significantly preceding ^{14}NO.

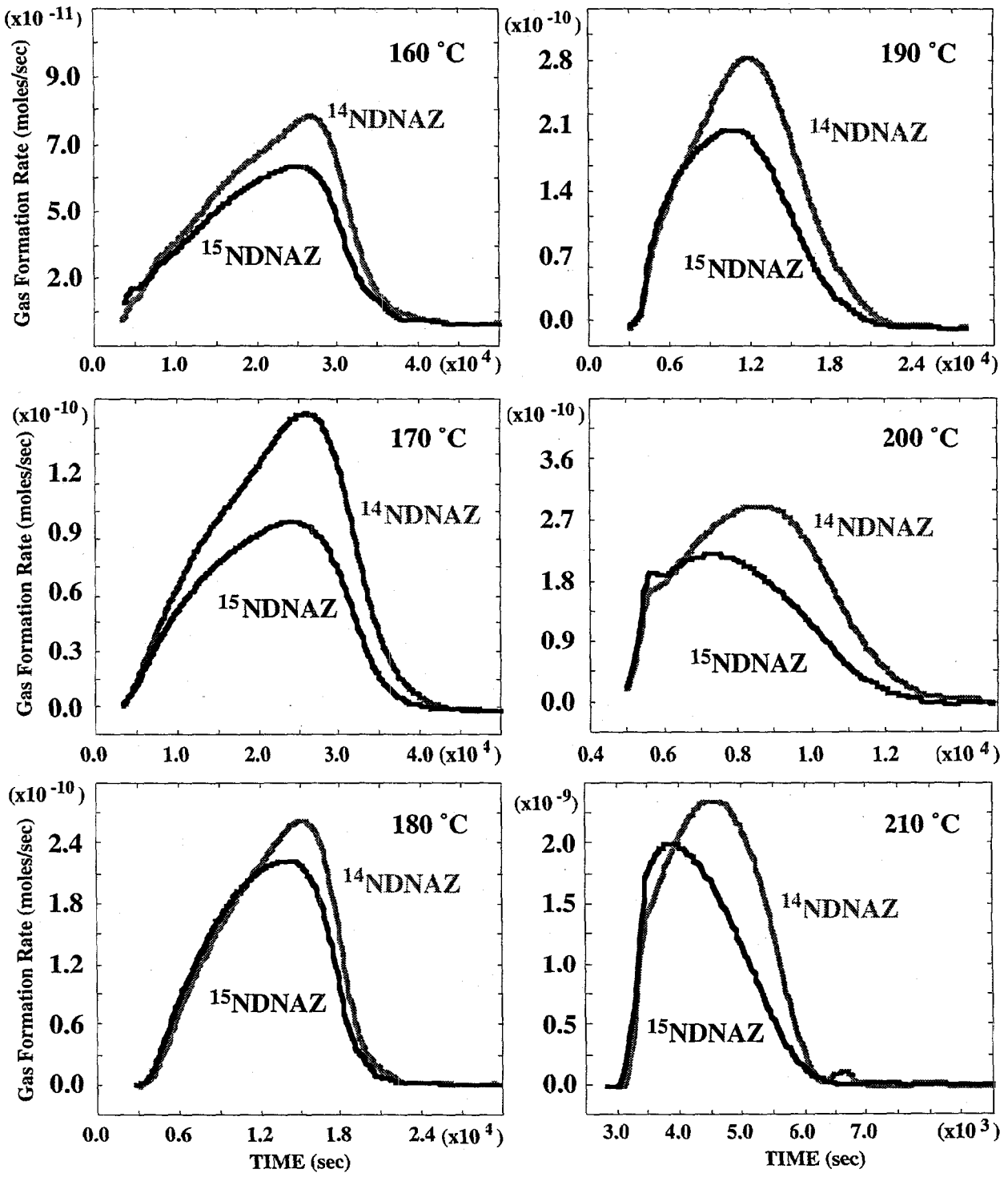

Figure 3: ^{15}NDNAZ and ^{14}NDNAZ formation in N-$^{15}NO_2$ labeled TNAZ decomposition. Note differing time behaviors. Also, as temperature increases, ^{15}NDNAZ formation begins to precede ^{14}NDNAZ formation.

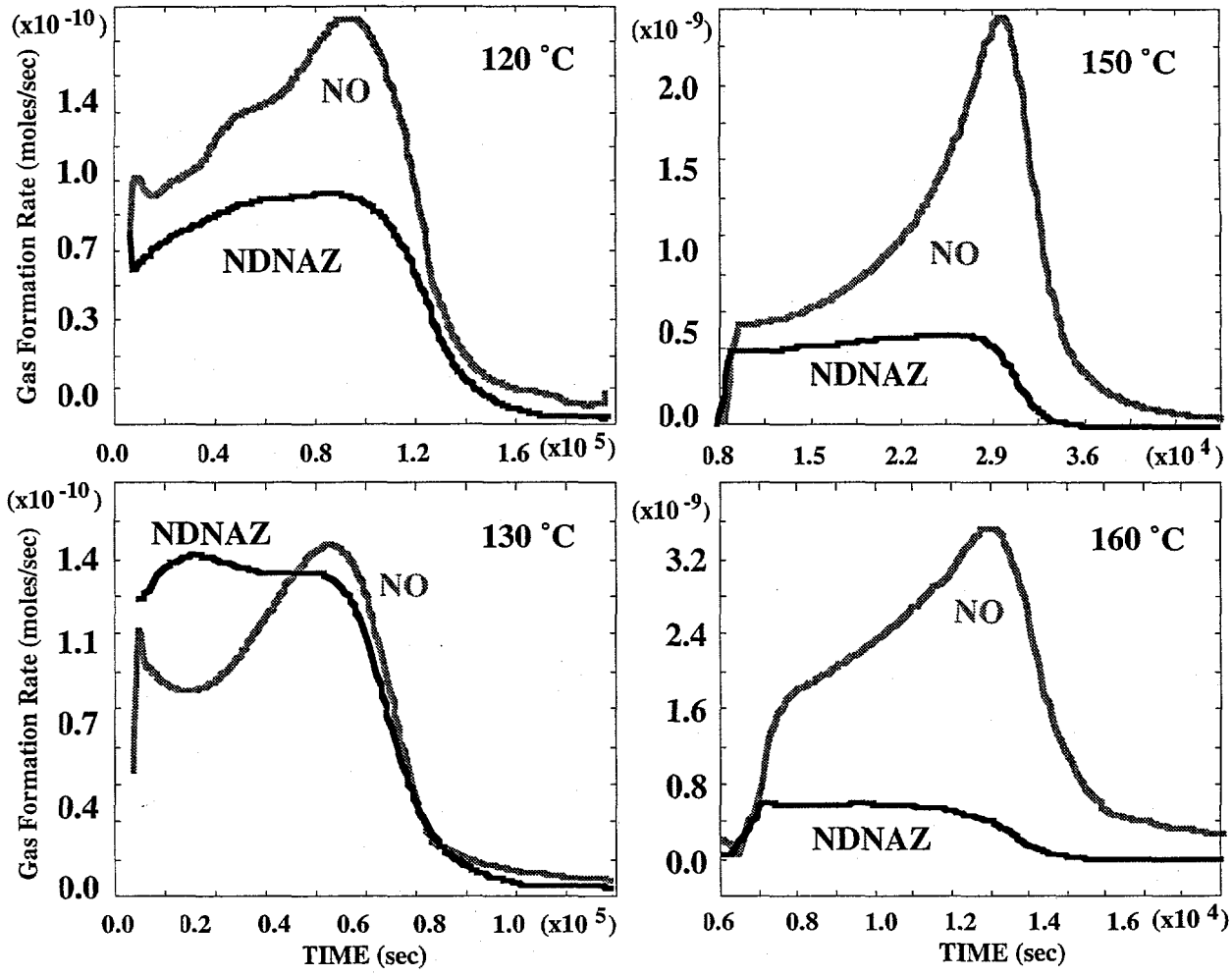

Figure 4: NO formation by decomposition of pure, independently synthesized NDNAZ. NO dominates at higher temperatures, indicating greater decomposition. The nonlinear increase in the NO rate over time is evidence of autocatalysis by the polymeric residue. More catalytic effect is evident in the 150°C experiment compared to the 160°C experiment because the 160°C sample is smaller (to avoid orifice blockage), and the NDNAZ is depleted before much residue is created.

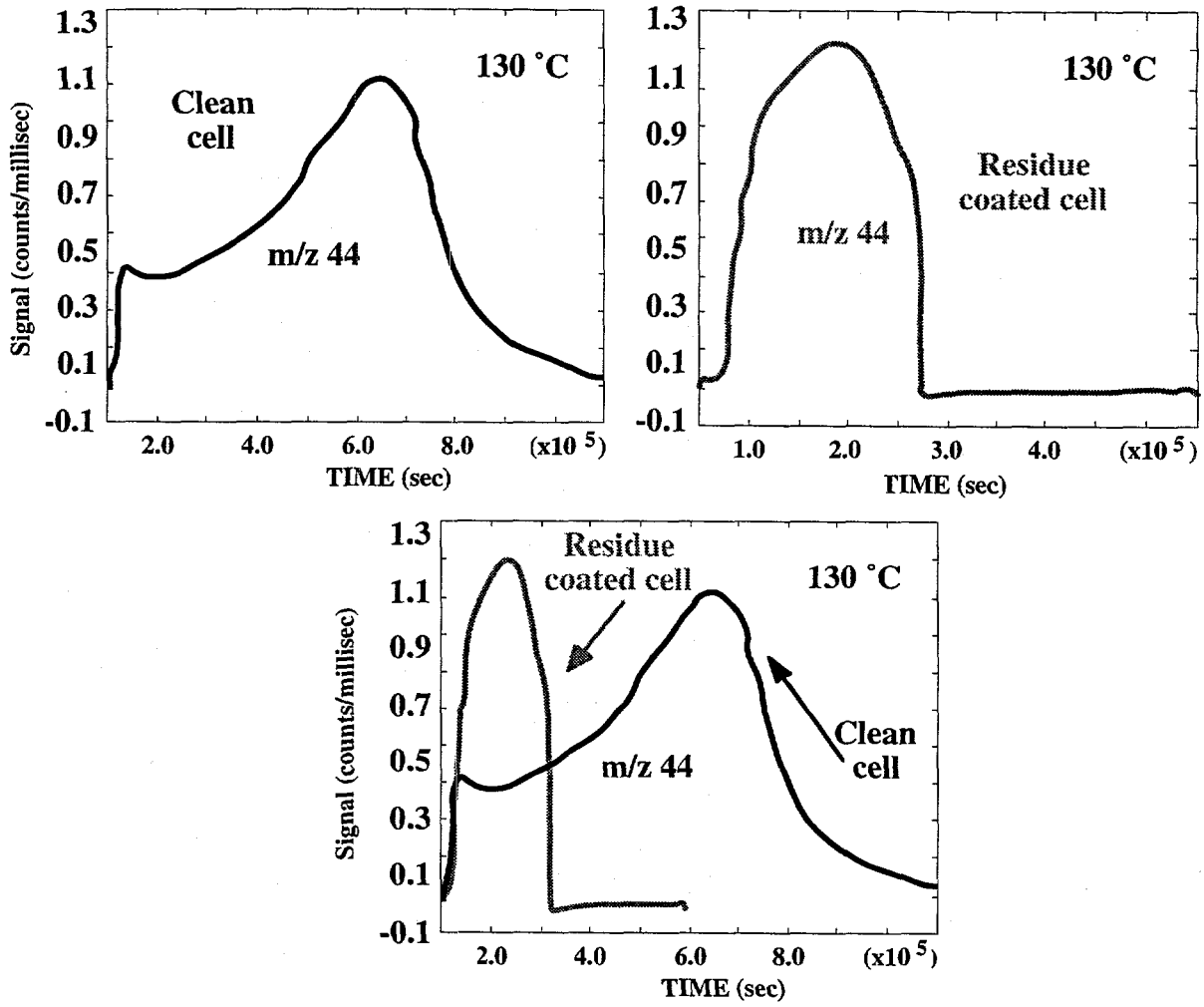

Figure 5: Proof that the autocatalytic behavior is due to the decomposition residue. Upper left, NDNAZ decomposition in a clean cell as monitored by m/z 44 (CO_2/N_2O). Upper right, fresh NDNAZ is added to the residue-coated cell and the rate of decomposition rises almost immediately to the peak rate from the previous experiment (and continues to increase). Lower middle shows the two signals superimposed at the same time scales. Note y axis here is ion signal, not gas formation rate.

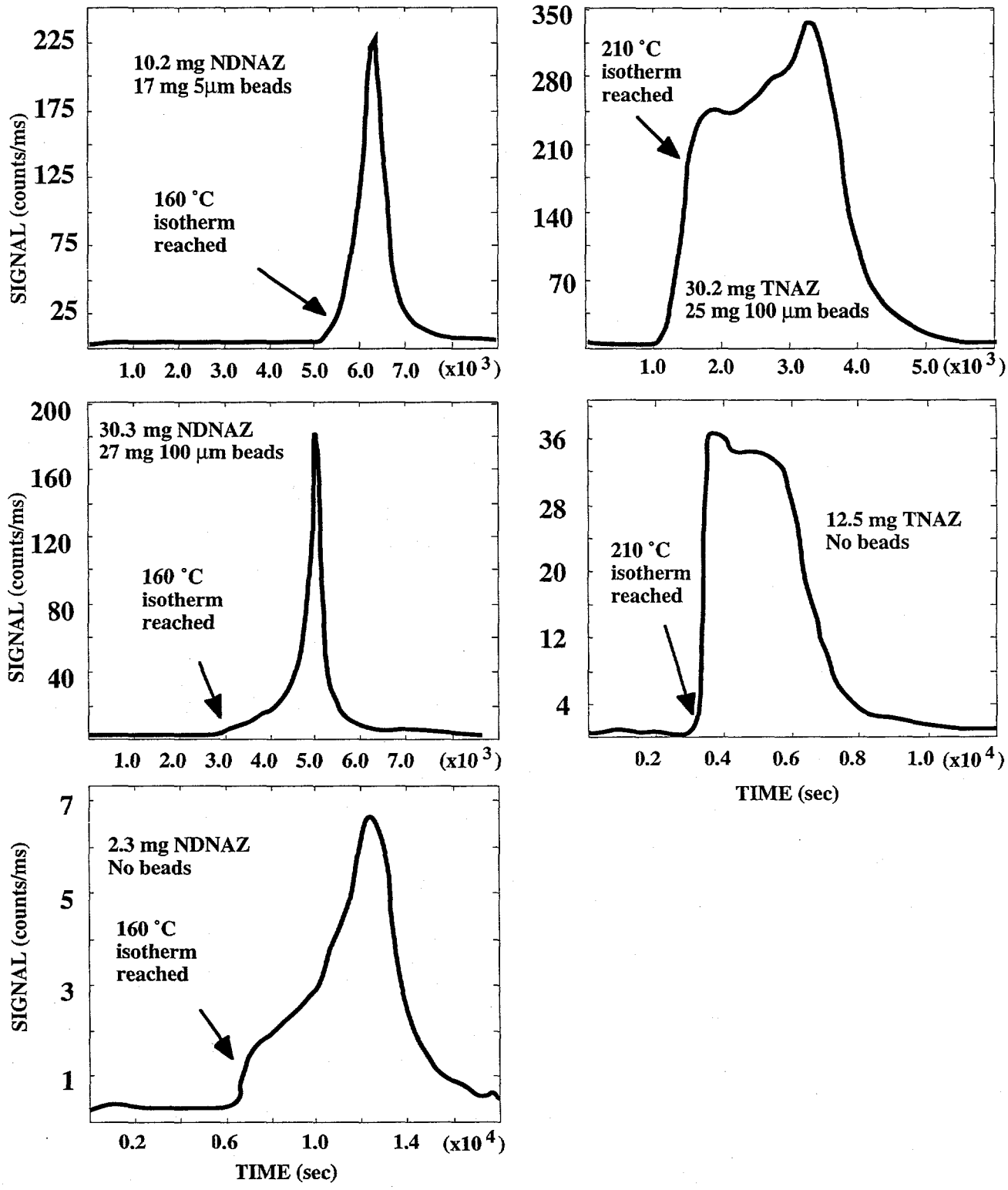

Figure 6: Higher rates of catalysis are see in the prescence of microscopic glass beads compared to normal decomposition. Left column, NDNAZ, right column, TNAZ. Note different time scales; the bead experiments for each compound are exactly half as long as the normal experiments. Also, note the > 2 order of magnitude increase in maximum ion signal with beads (again, m/z 44, CO_2/N_2O).

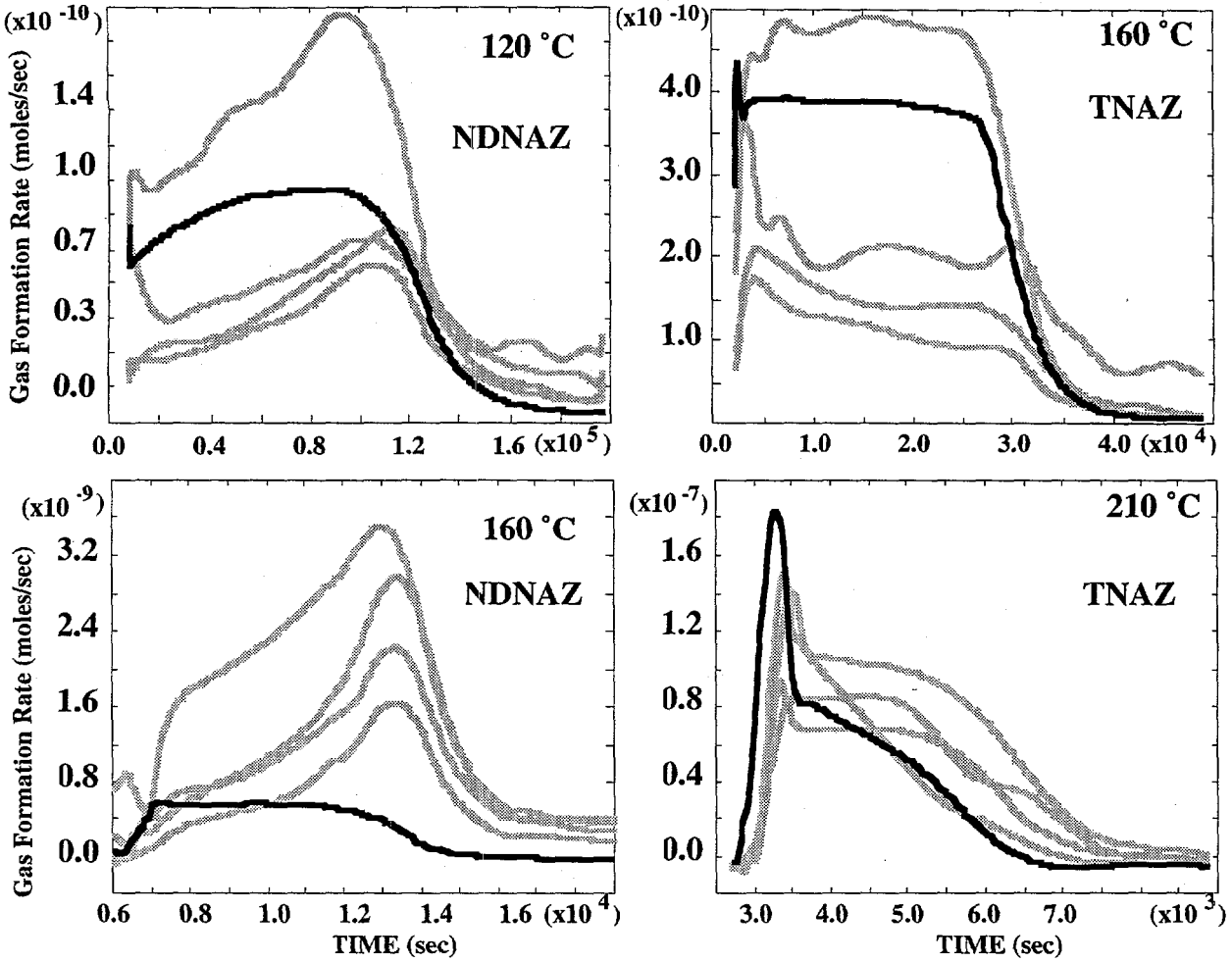

Figure 7: Evidence for less volatile intermediates and/or product trapping in polymeric residue. Dark lines represent the NDNAZ or TNAZ vapor formation rate, while grey lines represent various important low molecular weight products. In the top row, product evolution drops almost as soon as the parent material is depleted. At high temperature (bottom row), products continue to evolve after depletion.